Theory for current-induced intrinsic fieldlike spin-orbit torque in topological materials

Fu-Yang Chen,[1] Yi-Min Wang,[2] Yu-Chen Lin,[1] Hou-Jian Duan,[1,3] Ming-Xun Deng,[1,3,*] and Rui-Qiang Wang[1,3,†]

[1]*Guangdong Provincial Key Laboratory of Quantum Engineering and Quantum Materials, School of Physics, South China Normal University, Guangzhou 510006, China*

[2]*School of Teacher Education, Guangdong University of Education, Guangzhou 510303, China*

[3]*Guangdong-Hong Kong Joint Laboratory of Quantum Matter, Frontier Research Institute for Physics, South China Normal University, Guangzhou 510006, China*

(Received 13 April 2023; accepted 12 September 2023; published 25 September 2023)

The Berry curvature (BC), manifesting the band structure geometry, is extensively employed to describe the intrinsic transport properties, such as the intrinsic anomalous Hall effect and the spin Hall effect. The BC also can cause the intrinsic antidamping spin-orbit torque (SOT), but is regardless of the fieldlike SOT which is usually of extrinsic origins. Here, we study the current-induced SOT and reveal a new intrinsic fieldlike SOT in addition to the intrinsic antidamping SOT. The topological origin of the intrinsic SOTs can be understood with the BC defined in the mixed momentum-magnetization parameter space $(\boldsymbol{k}, \boldsymbol{M})$, rather than the conventional BC, which is especially important for systems with complicated spin-orbit interaction. We apply our theory to a magnetic semi-Dirac semimetal and find that the interplay between the peculiar spin textures and anisotropic band structure generates the intrinsic fieldlike SOT, which emerges even in the absence of band gap and for the Fermi energy far away from the Dirac points, quite different from the intrinsic antidamping SOT or anomalous Hall effect. Our findings provide another perspective to understand the physics of the current-induced SOTs.

DOI: 10.1103/PhysRevB.108.125140

I. INTRODUCTION

Spin-orbit torque (SOT), arising from the interaction between the nonequilibrium spin density of carriers and local magnetization, provides a promising mechanism of magnetization control for ferromagnetic or even antiferromagnetic layer proximity to spin-orbit-coupling systems with broken spatial inversion symmetry [1–10]. Due to the spin-momentum locking, when charge current passes through a system with spin-orbit interaction, the orbital angular momentum of the carriers can be transferred to their spin, leading to the nonequilibrium spin density, which in turn exerts a torque on the local magnetization via carrier-magnetic moment exchange coupling. These current-induced torques have been attracting great attention because they are believed to play a key role in the practical implementation of various spintronics concepts [11–21].

The SOT was observed experimentally early in epilayers of (Ga, Mn)As dilute magnetic semiconductors [3–5], later in several different metallic bilayers with structural inversion symmetry breaking [9–11,22–25], and recently in varied topological materials [26–31]. In analogy to the field and damping terms in the Landau-Lifshitz-Gilbert equation, the SOTs can be decomposed into fieldlike and dampinglike SOTs [2,31–33]. The current-induced SOTs can be examined by using the spin-torque ferromagnetic resonance (STFMR) [26,29,31] and the second-harmonic Hall measurement techniques [27,29,34]. In the STFMR measurement, the dampinglike and fieldlike components of the SOT can be extracted respectively from the symmetric and antisymmetric parts of the measured STFMR signal. Experimentally, a current-induced intrinsic antidamping SOT stemming from the Berry curvature (BC) was demonstrated [31] and has led to an explosion of activities in topological spintronics [12,13,15–21,31–33]. It is commonly believed that the BC, manifesting the band structure geometry, contributes to the intrinsic antidamping SOT with the same mechanism as in the intrinsic anomalous Hall effect (AHE) [35,36] and the spin Hall effect [37–39], but it is regardless of the fieldlike SOT which usually stems from extrinsic mechanisms. Interestingly, a recent study showed that in a single-domain ferromagnetic layer with Rashba spin-orbit coupling, the intrinsic SOT can be dominated by the fieldlike torque symmetry [40].

While the intrinsic antidamping SOT has been widely investigated in varied systems, a systematic theory for current-induced intrinsic fieldlike SOT with topological origin has not been established so far. In this work, we study the current-induced SOT based on the Green's function approach, and intriguingly find an extra intrinsic fieldlike SOT in addition to the usual intrinsic antidamping SOT. Both the intrinsic SOTs can be understood with a mixed Berry curvature, defined in the momentum-magnetization parameter space $(\boldsymbol{k}, \boldsymbol{M})$. We evaluate the intrinsic fieldlike SOT in a magnetic semi-Dirac semimetal (SDSM). Recently, the nonmagnetic [41–44] and magnetic [45,46] SDSMs have drawn a great deal of attention due to their unique band structure [47–52]: linear in one direction and quadratic in the orthogonal direction with different spin texture. We find that the intrinsic fieldlike SOT can survive for higher Fermi levels and even in the absence

*dengmingxun@scnu.edu.cn
†wangruiqiang@m.scnu.edu.cn

of band gap, in sharp contrast to the intrinsic dampinglike SOT [31].

The rest of this paper is organized as follows. In Sec. II, we introduce the model and theory. In Sec. III, we apply our theory to magnetic SDSMs, by which we reveal a new intrinsic fieldlike SOT in addition to the intrinsic antidamping SOT. The last section contains a short summary.

II. MODEL AND THEORY

We start from a system with general spin-orbit coupling, which is depicted by the Hamiltonian

$$\mathcal{H}(\boldsymbol{k}) = \boldsymbol{g}_{\boldsymbol{k}} \cdot \hat{\boldsymbol{\sigma}} + J\boldsymbol{M} \cdot \hat{\boldsymbol{s}}. \tag{1}$$

Here, $\hat{\boldsymbol{s}} = \hbar\hat{\boldsymbol{\sigma}}/2$ is the electron spin operator, $\hat{\boldsymbol{\sigma}} = (\hat{\sigma}_x, \hat{\sigma}_y, \hat{\sigma}_z)$ represents the vector of spin Pauli matrices and $\boldsymbol{M}$ denotes the magnetization of the adjacent ferromagnetic insulator (FMI). The spin-orbit interaction is dependent on the concrete form of $\boldsymbol{g}_{\boldsymbol{k}}$. Upon application of an external electric field, the linear-response function of the charge current and spin density can be combined into a unified formula (see Appendix A)

$$\chi_{j,ab} = -\frac{\hbar}{2\pi V}\int_{-\infty}^{\infty} d\epsilon \sum_{\boldsymbol{k}\mu\nu} \xi^{\mu a}_{\boldsymbol{k},j}\xi^{\nu b}_{\boldsymbol{k},1} \times \mathrm{Tr}\left[\hat{\sigma}_\mu G^<_{\boldsymbol{k}}\hat{\sigma}_\nu \partial_\epsilon G^A_{\boldsymbol{k}} - \hat{\sigma}_\mu \partial_\epsilon G^R_{\boldsymbol{k}}\hat{\sigma}_\nu G^<_{\boldsymbol{k}}\right], \tag{2}$$

where V is the volume of the sample and $\xi^{\mu a}_{\boldsymbol{k},j} = -\frac{e}{\hbar}\frac{\partial g_{\boldsymbol{k},\mu}}{\partial k_a}\delta_{j,1} + \frac{\hbar}{2}\delta_{\mu,a}\delta_{j,2}$, with (a, b) denoting the current direction and (μ, ν) denoting the spin direction, and $j = 1$ and 2 correspond respectively to the conductivity and torkance tensors, i.e., $\sigma_{ab} = \chi_{1,ab}$ and $\tau_{ab} = \chi_{2,ab}$. The relevant retarded/advanced Green's function is determined by

$$G^{R/A}_{\boldsymbol{k}} = \sum_{\eta=\pm}\frac{|\psi_{\boldsymbol{k},\eta}\rangle\langle\psi_{\boldsymbol{k},\eta}|}{\epsilon - \varepsilon_{\boldsymbol{k},\eta} \pm i\Gamma} = \frac{1}{2}\sum_{\eta=\pm}\frac{1}{\epsilon - \varepsilon_{\boldsymbol{k},\eta} \pm i\Gamma}\left(1 + \eta\frac{\boldsymbol{d}_{\boldsymbol{k}}}{|\boldsymbol{d}_{\boldsymbol{k}}|}\cdot\hat{\boldsymbol{\sigma}}\right), \tag{3}$$

with $\boldsymbol{d}_{\boldsymbol{k}} = \boldsymbol{g}_{\boldsymbol{k}} + J\hbar\boldsymbol{M}/2$, and $G^<_{\boldsymbol{k}} = (G^A_{\boldsymbol{k}} - G^R_{\boldsymbol{k}})f(\epsilon)$ defines the less Green's function, in which $\varepsilon_{\boldsymbol{k},\eta}$ denotes the eigenenergy of $\mathcal{H}(\boldsymbol{k})$ corresponding to the wavefunction $|\psi_{\boldsymbol{k},\eta}\rangle$, $\hbar/\Gamma$ represents the electron lifetime, and $f(\epsilon) = [1 + \exp(\frac{\epsilon - E_F}{k_B T})]^{-1}$ accounts for the Fermi-Dirac distribution function with chemical potential E_F and temperature T. The resulting nonequilibrium spin density $\Delta\boldsymbol{s} = (\tau_{xb}, \tau_{yb}, \tau_{zb})E_b$ will exert a torque $\boldsymbol{T} = \boldsymbol{M} \times \Delta\boldsymbol{s}$ on the adjacent FMI, with E_b being the magnitude of the electric field. According to the parity of $\Delta\boldsymbol{s}$ with respect to $\boldsymbol{M}$, the SOT can be separated into the fieldlike (even) and dampinglike (odd) components.

By substituting Eq. (3) into Eq. (2), we can divide the response function into the intraband contribution (see Appendix B)

$$\chi^{\mathrm{intra}}_{j,ab} = \frac{e}{V}\sum_{\boldsymbol{k}\eta,\mu\nu}\frac{1}{\Gamma}\frac{\partial f(\varepsilon_{\boldsymbol{k},\eta})}{\partial\varepsilon_{\boldsymbol{k},\eta}}\frac{d_{\boldsymbol{k},\mu}d_{\boldsymbol{k},\nu}}{|\boldsymbol{d}_{\boldsymbol{k}}|^2}\frac{\partial d_{\boldsymbol{k},\nu}}{\partial k_b}\xi^{\mu a}_{\boldsymbol{k},j} \tag{4}$$

and interband contributions

$$\chi^{\mathrm{inter},+}_{j,ab} = -\frac{\hbar}{V}\sum_{\boldsymbol{k}\eta,\mu\nu} f_{\boldsymbol{k},\eta}T^{\eta,+}_{\boldsymbol{k},\mu\nu}\xi^{\mu a}_{\boldsymbol{k},j}\xi^{\nu b}_{\boldsymbol{k},1}\sin 2\vartheta_{\boldsymbol{k}}, \tag{5}$$

$$\chi^{\mathrm{inter},-}_{j,ab} = -\frac{\hbar}{V}\sum_{\boldsymbol{k}\eta,\mu\nu} f_{\boldsymbol{k},\eta}T^{\eta,-}_{\boldsymbol{k},\mu\nu}\xi^{\mu a}_{\boldsymbol{k},j}\xi^{\nu b}_{\boldsymbol{k},1}\cos 2\vartheta_{\boldsymbol{k}}, \tag{6}$$

with $f_{\boldsymbol{k},\eta} = f(\varepsilon_{\boldsymbol{k},\eta})\cos^2\vartheta_{\boldsymbol{k}}$ and $\vartheta_{\boldsymbol{k}} = \cot^{-1}(2|\varepsilon_{\boldsymbol{k},\eta}|/\Gamma)$. Here, $T^{\eta,+}_{\boldsymbol{k},\mu\nu} = -\eta d_{\boldsymbol{k},\mu}d_{\boldsymbol{k},\nu}/(2|\boldsymbol{d}_{\boldsymbol{k}}|^4)$ originates from the Riemannian metric tensor [53], namely, the real part of the geometric tensor $\langle\frac{\partial\psi_{\boldsymbol{k},\eta}}{\partial d_{\boldsymbol{k},\mu}}|\frac{\partial\psi_{\boldsymbol{k},\eta}}{\partial d_{\boldsymbol{k},\nu}}\rangle$. $T^{\eta,-}_{\boldsymbol{k},\mu\nu}$ is relevant to the curvature tensor defined in the composite parameter space $\boldsymbol{R} = (\boldsymbol{k}, \boldsymbol{M})$, i.e.,

$$\Omega^{\eta}_{\boldsymbol{R},\mu\nu} = -\eta\frac{\boldsymbol{d}_{\boldsymbol{k}}}{2|\boldsymbol{d}_{\boldsymbol{k}}|^3}\cdot\left(\frac{\partial\boldsymbol{d}_{\boldsymbol{k}}}{\partial R_\mu}\times\frac{\partial\boldsymbol{d}_{\boldsymbol{k}}}{\partial R_\nu}\right), \tag{7}$$

the integral of which gives the generalized Chern number $\mathbb{C}^{\eta}_{\mu\nu} = (1/2\pi)\int\Omega^{\eta}_{\boldsymbol{R},\mu\nu}dR_\mu dR_\nu$. By replacing $R_{\mu,\nu} \to k_{\mu,\nu}$, Eq. (7) recovers the momentum-space BC $\Omega^{\eta}_{\boldsymbol{kk},\mu\nu}$. If replacing $R_\mu \to M_\mu$ and $R_\nu \to k_\nu$ in Eq. (7), one can obtain the mixed BC $\Omega^{\eta}_{\boldsymbol{Mk},\mu\nu}$, as defined in Refs. [32,33]. It can be verified that

$$\sum_{\mu\nu}T^{\eta,-}_{\boldsymbol{k},\mu\nu}\xi^{\mu a}_{\boldsymbol{k},j}\xi^{\nu b}_{\boldsymbol{k},1} = \frac{e^2}{\hbar^2}\Omega^{\eta}_{\boldsymbol{kk},ab}\delta_{j,1} - \frac{e}{2}\Omega^{\eta}_{\boldsymbol{Mk},ab}\delta_{j,2}. \tag{8}$$

Obviously, $\chi^{\mathrm{intra}}_{j,ab}$ and $\chi^{\mathrm{inter},+}_{j,ab}$ all contribute to the extrinsic SOT, while $\chi^{\mathrm{inter},-}_{j,ab}$ includes an intrinsic component independent of impurity scattering. To see more clearly the relation between the intrinsic SOTs and the curvature tensors, we can reduce Eq. (6) in the limit of $\Gamma \to 0$ or $\vartheta_{\boldsymbol{k}} \to 0$ as

$$\chi^{\mathrm{inter},-}_{j,ab} = -\frac{e}{V}\sum_{\boldsymbol{k}\eta}\left(\frac{e}{\hbar}\Omega^{\eta}_{\boldsymbol{kk},ab}\delta_{j,1} - \frac{\hbar}{2}\Omega^{\eta}_{\boldsymbol{Mk},ab}\delta_{j,2}\right)f(\varepsilon_{\boldsymbol{k},\eta}). \tag{9}$$

For systems with simple spin-orbit coupling, e.g., $\boldsymbol{g}_{\boldsymbol{k}}$ is linear in $\boldsymbol{k}$, $\Omega^{\eta}_{\boldsymbol{kk},ab}$ differs from $\Omega^{\eta}_{\boldsymbol{Mk},ab}$ only by a constant factor. This may lead one to an incorrect conclusion that the momentum-space BC is responsible for the intrinsic SOTs. In fact, according to Eq. (9), the intrinsic SOTs, encoded in the torkance tensor $\chi^{\mathrm{inter},-}_{2,ab}$, should be characterized by the mixed BC. Indeed, the momentum-space BC fails to capture the intrinsic SOTs in systems with complicated spin-orbit interaction, such as the magnetic SDSM studied below.

III. INTRINSIC FIELDLIKE SOT IN MAGNETIC SDSMs.

Specifically, we consider a minimal model for the magnetic SDSMs [45,46], where the spin-orbit coupling takes the form $\boldsymbol{g}_{\boldsymbol{k}} = (\alpha k_x^2 - \delta_0, \upsilon k_y, 0)$. For convenience of discussion, we use the dimensionless parameters and assume α and υ to be positive. Specifically, for a typical SDSMs, the system parameters can be $\alpha = 7.5$ meV nm^2, $\upsilon = 65$ meV nm and the gap parameter varied from $\delta_0 = 1$ meV to 10 meV, as taken in Refs. [54,55]. Similar magnetic SDSM model has been employed as the ferromagnetic layers of the ferromagnetic/normal metal/ferromagnetic sandwich structure, where the spin current density and spin-transfer torques were studied [45]. As the sample is attached to a FMI, $\boldsymbol{d}_{\boldsymbol{k}} = (\alpha k_x^2 - \delta_0', \upsilon k_y', M_z)$ and we can obtain the dispersion

$$\varepsilon_{\boldsymbol{k},\eta} = \eta\sqrt{\left(\alpha k_x^2 - \delta_0'\right)^2 + \upsilon^2 k_y'^2 + M_z^2} \tag{10}$$

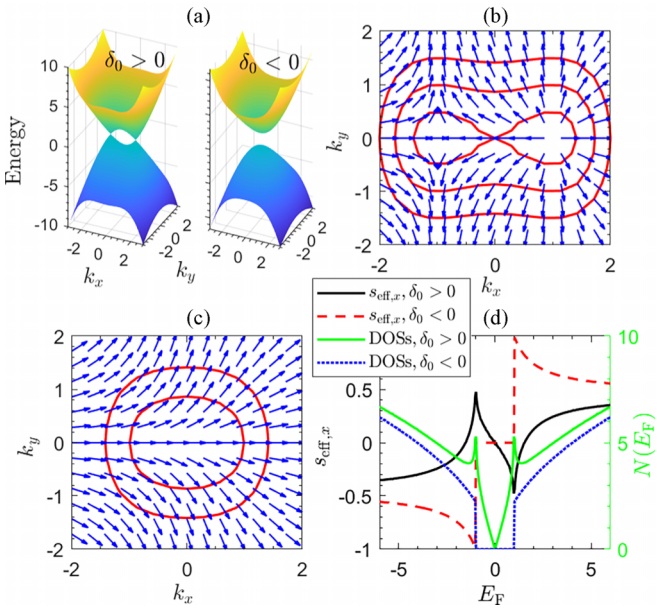

FIG. 1. (a) The dispersion of the ferromagnetic SDSM without FMI for $\delta_0 > 0$ in the left panel and $\delta_0 < 0$ in the right panel, whose conduction band's spin textures are displayed in (b) and (c), respectively, where the red curves represent the energy contour. (d) The averaged spin polarization (left axis) and DOSs (right axis) vs E_F, where the vanishing $s_{\text{eff},y}$ and $s_{\text{eff},z}$ components are not shown.

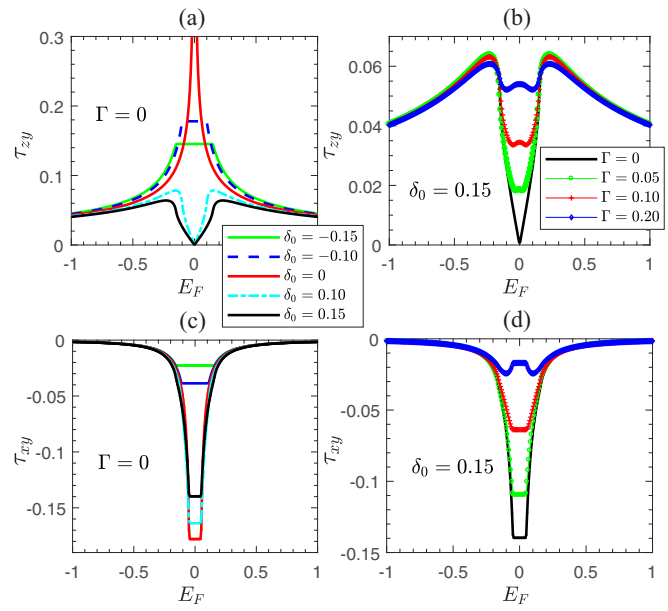

FIG. 2. The torkance tensor elements τ_{zy} (the first row) and τ_{xy} (the second row) in units of $e\hbar/2$ vs E_F for different δ_0 (Γ) in the first (second) column. Here, we set [(a)–(b)] $M_z = 0$ and [(c)–(d)] $M_z = 0.05$. Other parameters are set as $\upsilon = 1$, $\alpha = 2$, $k_BT = 0.001$, and $M_{x,y} = 0$.

and the corresponding wavefunction

$$|\psi_{\boldsymbol{k},\eta}\rangle = \frac{1}{\sqrt{2\varepsilon_{\boldsymbol{k},\eta}(\varepsilon_{\boldsymbol{k},\eta} - d_{\boldsymbol{k},z})}} \begin{pmatrix} d_{\boldsymbol{k},x} - id_{\boldsymbol{k},y} \\ \varepsilon_{\boldsymbol{k},\eta} - d_{\boldsymbol{k},z} \end{pmatrix}, \tag{11}$$

where $\delta_0' = \delta_0 - M_x$, $k_y' = k_y + M_y/\upsilon$, and $\eta = \pm$ indexes the conduction/valence band. In Fig. 1(a), we plot the dispersion for the SDSM, from which we see that the spectrum is parabolic/linear in the x/y direction. In equilibrium, the nontrivial spin texture $\boldsymbol{s}^\eta(\boldsymbol{k}) \equiv \langle\psi_{\boldsymbol{k},\eta}|\hat{\boldsymbol{s}}|\psi_{\boldsymbol{k},\eta}\rangle = \eta\hbar\boldsymbol{d}_{\boldsymbol{k}}/(2|\boldsymbol{d}_{\boldsymbol{k}}|)$, as displayed in Figs. 1(b) and 1(c), can result in net magnetization for the magnetic SDSM, which can be captured by the averaged spin density over the Fermi surface

$$\boldsymbol{s}_{\text{eff}} = \frac{1}{N(E_F)} \sum_{\boldsymbol{k}\eta} \boldsymbol{s}^\eta(\boldsymbol{k}) \delta(\varepsilon_{\boldsymbol{k},\eta} - E_F). \tag{12}$$

Here, $N(E_F) = \sum_{\boldsymbol{k}\eta} \delta(\varepsilon_{\boldsymbol{k},\eta} - E_F)$ is the density of states (DOSs) at the Fermi level. The averaged spin density and DOSs vs E_F are shown in Fig. 1(d).

In the absence of the FMI, the conduction and valence bands touch at $\boldsymbol{K}_\pm = (\pm\sqrt{\delta_0/\alpha}, 0)$ for $\delta_0 > 0$, forming a pair of 2D Dirac points. From Eq. (10), we see that the y-component magnetization M_y of the FMI will shift the Dirac points in the y direction and the other two components $M_{x,z}$ can open gap for the spectrum. The ways of the gap-opening effect of M_x and M_z are quite different. By tuning M_x, the Dirac points with decreasing δ_0' will come closer and merge at $\delta_0 = M_x$ and further be gapped out for $\delta_0 < M_x$, while a finite M_z gaps the spectrum without moving the Dirac points. The gap closing and reopening imply a topological phase transition process. Unfortunately, the varied topological phases here cannot be distinguished well by the Chern number of the momentum-space BC. The momentum-space BC is given by $\Omega^\eta_{\boldsymbol{kk},ab} = -\varepsilon^{ab\bar{z}} M_z \upsilon\alpha k_x/\varepsilon^3_{\boldsymbol{k},\eta}$, which is odd in k_x, with ε^{abc} being the 3D antisymmetric tensor. As a result, the Chern number $C^\eta = (1/2\pi)\int \Omega^\eta_{\boldsymbol{kk},xy} dk_x dk_y = 0$.

Instead, the topology of the SDSMs can be captured by the mixed BC defined in Eq. (7), which is specifically given by $\Omega^\eta_{\boldsymbol{Mk},zy} = \eta\hbar\upsilon(\alpha k_x^2 - \delta_0')/(4|\boldsymbol{d}_{\boldsymbol{k}}|^3)$ and $\Omega^\eta_{\boldsymbol{Mk},xy} = -\eta\hbar\upsilon M_z/(4|\boldsymbol{d}_{\boldsymbol{k}}|^3)$. As a result, the mixed Chern numbers, which describes the flux of the mixed BC through the M_a-k_b plane for constant k_c, read as $\mathbb{C}^\eta_{zy}(k_x) = \frac{\eta}{2}\text{sgn}(\alpha k_x^2 - \delta_0')$ and $\mathbb{C}^\eta_{xy}(k_x) = -\frac{\eta}{2}\text{sgn}(M_z)$, similar to the scenario in Weyl semimetals [56–58] . Thus, finite torkance τ_{zy} and τ_{xy} can be obtained from the second term in Eq. (9). This implies that in study of the current-induced spin polarization or intrinsic SOT in the SDSMs, one must use the mixed BC rather than the conventional BC.

Notice that the leading term of $\Omega^\eta_{\boldsymbol{Mk},xy}$ is proportional to $\boldsymbol{M}$ while the leading term of $\Omega^\eta_{\boldsymbol{Mk},zy}$ is independent of $\boldsymbol{M}$. According to the definition $\boldsymbol{T} = \boldsymbol{M} \times \Delta\boldsymbol{s}$, the torkance τ_{xy} contributes to the intrinsic antidamping SOT and τ_{zy} to the intrinsic fieldlike SOT. Next, we compare other differences between the torkance τ_{xy} and τ_{zy}. First, $\tau_{xy} \propto M_z$ only survives for finite band gap with $M_z \neq 0$, which recalls the scenario for the momentum-space BC induced intrinsic antidamping SOT as in literature [31,59] or intrinsic AHE [35,36]. Differently, τ_{zy} can emerge even in the absence of band gap with $M_z = 0$. The numerical results of the torkance τ_{zy} are plotted in Figs. 2(a) and 2(b). As expected, the mixed BC can induce intrinsic nonequilibrium spin density even for $M_z = 0$. As shown by Fig. 2(a), if $\delta_0 < 0$, τ_{zy} exhibits a plateau when $|E_F| < |\delta_0|$, whose height is $\sim 1/\sqrt{\alpha|\delta_0|}$ and width $\sim 2|\delta_0|$, while if $\delta_0 > 0$, the plateau turns to a valley with $\tau_{zy} = 0$ at the

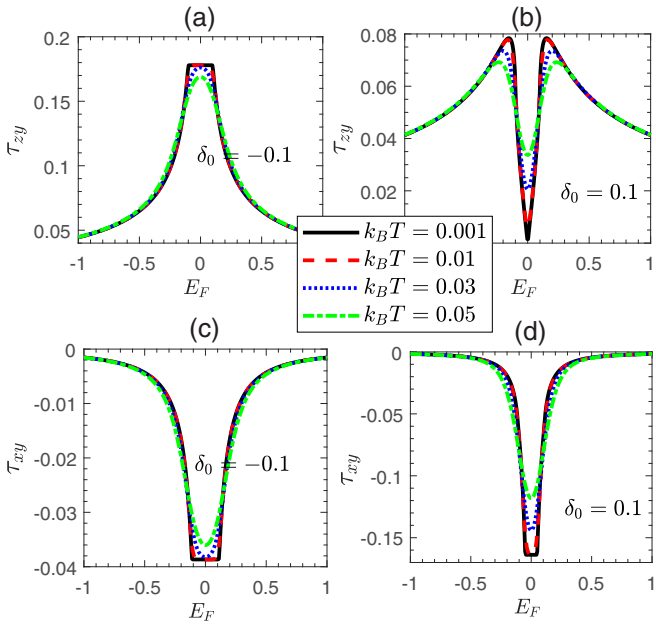

FIG. 3. Evolution of the torkance tensor elements τ_{zy} and τ_{xy} with temperature, in which $\Gamma = 0$ and other parameters are the same as Fig. 2.

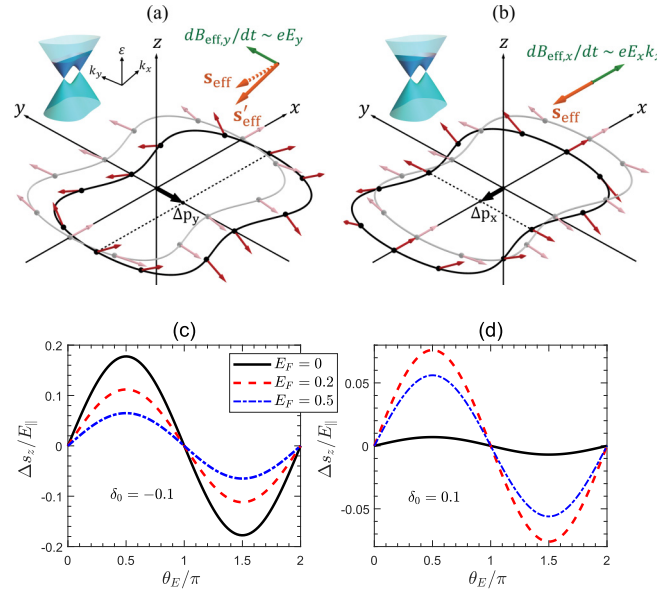

FIG. 4. Schematic of the current-induced nonequilibrium spin density for the electric field (green arrows) applied in the (a) y direction and (b) x direction. The semitransparent regions represent the equilibrium configuration, where the dark solid curves denote the energy contour and the red arrows thereon indicate the spin direction. The interband contribution can be attributed to intrinsic magnetization of the band, in which the carrier spins experience an equilibrium effective magnetic field $\boldsymbol{B}_{\text{eff}} = (B_{\text{eff},x}, 0, 0)$ and the electrons possess an effective spin polarization $\boldsymbol{s}_{\text{eff}} = (s_{\text{eff},x}, 0, 0)$, denoted by the red dotted arrow. For (a) $\boldsymbol{E} = E_y\hat{e}_y$, during electron acceleration in the electric field, the effective magnetic field acquires a time-dependent y component with $dB_{\text{eff},y}/dt \sim eE_y$, which rotates the spin from $\boldsymbol{s}_{\text{eff}}$ to $\boldsymbol{s}'_{\text{eff}}$, and (b) $\boldsymbol{E} = E_x\hat{e}_x$, $dB_{\text{eff},x}/dt \sim eE_xk_x$ is parallel to $\boldsymbol{s}_{\text{eff}}$ and thus can not rotate $\boldsymbol{s}_{\text{eff}}$. (c)−(d) Dependence of the intrinsic torkance $\tau_{z\parallel} = \Delta s_z/E_\parallel$ on the angle of the in-plane electric field $\boldsymbol{E} = E_\parallel(\cos\theta_E\hat{e}_x + \cos\sin\theta_E\hat{e}_y)$ for varied E_F, with (c) $\delta_0 = -0.1$, (d) $\delta_0 = 0.1$, and the rest of the parameters are set the same as Fig. 2(a).

Dirac points $E_F = 0$. Only for $M_z \neq 0$, nonzero τ_{xy} emerges as shown in Fig. 2(c), in which the curves are also sensitive to the SDSM parameter δ_0 within the band gap. With E_F away from the Dirac points, τ_{xy} tends to vanish but τ_{zy} remains finite.

Physically, the current-induced intrinsic nonequilibrium spin density and the related intrinsic fieldlike SOT can be understood from Figs. 4(a) and 4(b). In equilibrium, the magnetic SDSM possesses finite magnetization in direction x, see Fig. 1(d), such that the electrons experience an effective magnetic field $\boldsymbol{B}_{\text{eff}} = (B_{\text{eff},x}, 0, 0)$ and are magnetized effectively along the x direction with $\boldsymbol{s}_{\text{eff}} = (s_{\text{eff},x}, 0, 0)$. During acceleration in the electric field $\boldsymbol{E}$, the effective magnetic field the electrons feel, because of the spin-momentum locking in $\boldsymbol{g}_{\boldsymbol{k}} \cdot \hat{\boldsymbol{\sigma}}$, will acquire a time-dependent component, with $\partial_t B_{\text{eff},x} = -2eE_x\alpha k_x/(g\mu_B\hbar)$ and $\partial_t B_{\text{eff},y} = -eE_y\upsilon/(g\mu_B\hbar)$, where g and μ_B denote the g factor and Bohr magneton, respectively. Then, by solving the Bloch equations for $\boldsymbol{s}_{\text{eff}}$, i.e.,

$$\frac{d\boldsymbol{s}_{\text{eff}}}{dt} = \frac{1}{\hbar}\boldsymbol{s}_{\text{eff}} \times \boldsymbol{B}_{\text{eff}}, \tag{13}$$

we obtain

$$\Delta s_{\text{eff},a} \simeq \frac{\hbar\varepsilon^{abc}}{|\boldsymbol{B}_{\text{eff}}|^2}\left(s_{\text{eff},b}\frac{dB_{\text{eff},c}}{dt} - s_{\text{eff},c}\frac{dB_{\text{eff},b}}{dt}\right). \tag{14}$$

In fact, the mixed BC in Eq. (7) is closely related to the spin texture, which can be written as

$$\Omega^{\eta}_{\boldsymbol{M}\boldsymbol{k},ab} = -\frac{\varepsilon^{abc}}{2|\boldsymbol{d}_{\boldsymbol{k}}|^2}\frac{\partial d_{\boldsymbol{k},b}}{\partial k_b}s^{\eta}_c(\boldsymbol{k}). \tag{15}$$

This implies that the spin polarization $\boldsymbol{s}_{\text{eff}}$ is crucial for the current-induced intrinsic fieldlike SOT. For $M_z = 0$, we find $\tau_{zy} \sim \Delta s_{\text{eff},z}/E_y = -\frac{e\upsilon}{g\mu_B}\frac{s_{\text{eff},x}}{|\boldsymbol{B}_{\text{eff}}|^2}$ is finite for $\boldsymbol{E} = E_y\hat{e}_y$, while $\tau_{zx} \sim \Delta s_{\text{eff},z}/E_x = 0$ for $\boldsymbol{E} = E_x\hat{e}_x$.

If $M_z \neq 0$, the band electrons will be out-of-plane magnetized by the FMI, namely, $s_{\text{eff},z}$ is nonvanishing. In this case, $\Delta s_{\text{eff},x} = \frac{e\upsilon}{g\mu_B}\frac{s_{\text{eff},z}}{|\boldsymbol{B}_{\text{eff}}|^2}E_y$ and $\Delta s_{\text{eff},y} = -\frac{2e\alpha}{g\mu_B}\frac{s_{\text{eff},z}}{|\boldsymbol{B}_{\text{eff}}|^2}k_xE_x$. Therefore, a finite x component intrinsic nonequilibrium spin density can be induced, while the net y-component nonequilibrium spin density vanishes, because $\Delta s_{\text{eff},y}$ is odd in k_x. Here, $\tau_{xy} \propto M_z$ is of dampinglike property, while τ_{zy} can be $\boldsymbol{M}$ independent, demonstrating its fieldlike nature.

From above discussions, one can notice that the mixed BC induced SOTs only include the intrinsic antidamping SOT $\sim\tau_{xy}$ and intrinsic fieldlike SOT $\sim\tau_{zy}$, and other transverse and all longitudinal components are vanishing. Except for the intrinsic components, there are some extrinsic components $\chi^{\text{intra}}_{j,ab}$, $\chi^{\text{inter},+}_{j,ab}$ and partly in $\chi^{\text{inter},-}_{j,ab}$, which depend heavily on the impurity scattering characterized by a finite Γ, see Figs. 2(b) and 2(d). From analysis of the parity (see Appendix C), we find that both $\chi^{\text{intra}}_{j,ab}$ and $\chi^{\text{inter},+}_{j,ab}$ are zero for $a \neq b$, namely, they possess only longitudinal components. The evolution of the intrinsic torkance tensor elements τ_{zy} and τ_{xy} with temperature is displayed in Fig. 3, which indicates

that, due to the broadening effect of the Fermi surface by the thermal fluctuation, the SOTs can be sensitive to temperature when the Fermi level is near the Dirac point. As a result of the anisotropic spin texture of the magnetic SDSMs, the nonequilibrium spin density is maximum (vanishing) when the current flows in the linear (parabolic) direction. This leads to the sine dependence of the current-induced nonequilibrium spin density on the direction of the electric field, as illustrated by Figs. 4(c) and 4(d). Additionally, the spin texture of the magnetic SDSMs not only relies strongly on the model parameter δ_0 and the Fermi energy, but also can be modulated by the FMI, and as a result, the intrinsic fieldlike SOT can be tunable magnetically and electrically. In experiments, it is expected that the intrinsic fieldlike SOT would be observable in magnetic topological materials by the STFMR technique, which can be extracted from the antisymmetric part of the STFMR signal [26,29,31]. The intrinsic and extrinsic contributions can be distinguished by the doping or disordered effects.

IV. SUMMARY

In conclusion, we have derived a formula for the current-induced intrinsic SOTs and find that the topological origin of the intrinsic SOTs can be captured with the mixed BC, rather than the momentum-space BC responsible for the intrinsic AHE. In systems with simple spin-orbit coupling, the results from the mixed BC can recover those from the momentum-space BC. However, for systems with complicated spin-orbit coupling, the mixed BC predicts the existence of current-induced intrinsic fieldlike SOT, which is beyond the description of the momentum-space BC. We apply our theory to a magnetic SDSM model and find it displays both the intrinsic dampinglike and intrinsic fieldlike SOTs owing to the interplay between the peculiar spin textures and anisotropic band structure. Furthermore, these two types of intrinsic SOTs exhibit different dependence on the band gap and E_F. We expect the intrinsic fieldlike SOT to be observable in magnetic topological materials.

ACKNOWLEDGMENTS

This work was supported by the National Natural Science Foundation of China under Grants No. 12274146, No. 11874016, No. 12174121, and No. 12104167, the Guangdong Basic and Applied Basic Research Foundation under Grant No. 2023B1515020050, the Guangzhou Basic and Applied Basic Research Foundation under Grant No. 202102020556, the Science and Technology Program of Guangzhou under Grant No. 2019050001, and the Guangdong Provincial Key Laboratory under Grant No. 2020B1212060066. F.-Y.C. and Y.-M.W. contributed equally to this work.

APPENDIX A: LINEAR-RESPONSE THEORY: A GREEN'S FUNCTION APPROACH

Let us start from a general Hamiltonian $\mathcal{H}_0$, which is driven by external perturbation $H'(t)$. The expectation of a mechanical quantity denoted by operator $\hat{Q}$ can be expressed as

$$Q(t) = \mathrm{Tr}[U^\dagger(t,-\infty)\hat{Q}(t)U(t,-\infty)\hat{\rho}_0], \tag{A1}$$

where $\hat{Q}(t) = e^{\frac{i}{\hbar}\mathcal{H}_0 t}\hat{Q}e^{-\frac{i}{\hbar}\mathcal{H}_0 t}$, $\hat{\rho}_0$ denotes the unperturbed density matrix, and

$$U(t,-\infty) = \hat{\mathcal{T}}\exp\left(\frac{1}{i\hbar}\int_{-\infty}^{t} dt'\hat{H}'(t')\right) \tag{A2}$$

represents the time-evolution operator in the interaction picture. Here, $\hat{H}'(t) = e^{\frac{i}{\hbar}\mathcal{H}_0 t}H'(t)e^{-\frac{i}{\hbar}\mathcal{H}_0 t}$ and $\hat{\mathcal{T}}$ is the time-ordering operator. In the spirit of the linear-response theory, we can write $Q(t) = Q_0 + \Delta Q(t)$, where $Q_0 = \mathrm{Tr}(\hat{Q}\hat{\rho}_0)$ and

$$\Delta Q(t) = -\frac{i}{\hbar}\int_{-\infty}^{t} dt'\Theta(t-t')\mathrm{Tr}\langle[\hat{Q}(t),\hat{H}'(t')]\rangle \tag{A3}$$

accounts for the linear response of $\hat{Q}$ to perturbation $H'(t)$, in which $\Theta(x)$ is the Heaviside function.

Usually, the correlation function in Eq. (A3) can be evaluated by means of the Matsubara Green's function, during which time one will encounter complicated Matsubara frequency summation. Below, we calculate Eq. (A3) directly by the common retarded and advanced Green's functions, which does not involve complicated contour integral. The matrix elements of the retarded/advanced Green's function are defined as

$$G^{R/A}_{\mu\nu}(t,t') = \pm\Theta(\pm t \mp t')[G^{>}_{\mu\nu}(t,t') - G^{<}_{\mu\nu}(t,t')], \tag{A4}$$

where the less and greater Green's functions are given by

$$G^{<}_{\mu\nu}(t,t') = i\langle c^\dagger_\nu(t')c_\mu(t)\rangle/\hbar, \tag{A5}$$

$$G^{>}_{\mu\nu}(t,t') = -i\langle c_\mu(t)c^\dagger_\nu(t')\rangle/\hbar. \tag{A6}$$

Here, $c^\dagger_\mu(t)$ and $c_\mu(t)$ are the electron creation and annihilation operators, acting on a set of complete basis vectors, saying $\{|\psi_\mu\rangle\}$. Then, in the Hilbert space $\{|\psi_\mu\rangle\}$, we can express Eq. (A3) as

$$\Delta Q(t) = -i\hbar\int_{-\infty}^{t} dt'\Theta(t-t')\sum_{\mu\nu\lambda\gamma} Q_{\mu\nu}H'_{\lambda\gamma}(t') \times [G^{>}_{\nu\lambda}(t,t')G^{<}_{\gamma\mu}(t',t) - G^{<}_{\nu\lambda}(t,t')G^{>}_{\gamma\mu}(t',t)], \tag{A7}$$

where $Q_{\mu\nu} = \langle\psi_\mu|\hat{Q}|\psi_\nu\rangle$ and $H'_{\lambda\gamma}(t') = \langle\psi_\lambda|H'(t')|\psi_\gamma\rangle$. For convenience, one can choose the eigenstates of $\mathcal{H}_0$ as the basis of the Hilbert space, such that the Green's functions contain only the diagonal elements. However, it should be noted that this is not the only choice, because the basis will be traced out and the final result is representation independent. By substituting Eq. (A4) into Eq. (A7), we can derive for

$$\Delta Q(t) = -i\hbar\int_{-\infty}^{t} dt'\mathrm{Tr}[\hat{Q}(t)G^{<}(t,t')H'(t') \times G^{A}(t',t) + \hat{Q}(t)G^{R}(t,t')H'(t')G^{<}(t',t)] \tag{A8}$$

which can be re-expressed as

$$\Delta Q(t) = \frac{1}{2\pi}\int_{-\infty}^{\infty} d\omega e^{-i\omega t}\Delta Q(\omega), \tag{A9}$$

where

$$\Delta Q(\omega) = \frac{-i}{2\pi}\int_{-\infty}^{\infty} d\epsilon \mathrm{Tr}[\hat{Q}G^{<}(\epsilon)H'(\omega) \times G^{A}(\epsilon-\hbar\omega) + \hat{Q}G^{R}(\epsilon+\hbar\omega)H'(\omega)G^{<}(\epsilon)], \tag{A10}$$

with $G^{<}(\epsilon) = [G^{A}(\epsilon) - G^{R}(\epsilon)]f(\epsilon)$ defining the less Green's function. Here, $H'(\omega)$ denotes the Fourier transform of $H'(t')$ and $f(\epsilon) = [1+\exp(\frac{\epsilon-E_F}{k_BT})]^{-1}$ is the Fermi-Dirac distribution function.

When an ac electric field $E_b(\boldsymbol{r},t) = E_b e^{-i(\boldsymbol{q}\cdot\boldsymbol{r}-\omega t)}$ is applied to the sample, the perturbation Hamiltonian takes the form

$$H'(\omega) = i\omega^{-1}\int d^3\boldsymbol{r}\hat{\jmath}_b(\boldsymbol{r})E_b e^{-i\boldsymbol{q}\cdot\boldsymbol{r}}, \tag{A11}$$

where $\hat{\jmath}_b$ denotes the current density operator. For $\omega\to 0$, we can approximate $G^{A}(\epsilon-\hbar\omega)\simeq G^{A}(\epsilon)-\partial_\epsilon G^{A}(\epsilon)\hbar\omega$ and $G^{R}(\epsilon+\hbar\omega)\simeq G^{R}(\epsilon)+\partial_\epsilon G^{R}(\epsilon)\hbar\omega$, such that Eq. (A10) becomes

$$\Delta Q(\omega) = \frac{i\hbar\omega}{2\pi}\int_{-\infty}^{\infty} d\epsilon \mathrm{Tr}[\hat{Q}G^{<}(\epsilon) \times H'(\omega)\partial_\epsilon G^{A}(\epsilon) - \hat{Q}\partial_\epsilon G^{R}(\epsilon)H'(\omega)G^{<}(\epsilon)], \tag{A12}$$

where an imaginary term $\sim i\mathrm{Tr}[\hat{Q}G^{<}(\epsilon)H'(\omega)G^{A}(\epsilon)+\hat{Q}G^{R}(\epsilon)H'(\omega)G^{<}(\epsilon)]$ was dropped. By replacing $\hat{Q}\to\hat{Q}_a$ and $H'(\omega)$ in Eq. (A12), we can arrive at

$$\chi_{ab} = -\frac{\hbar}{2\pi V}\int_{-\infty}^{\infty} d\epsilon \mathrm{Tr}[\hat{Q}_a G^{<}(\epsilon)\hat{\jmath}_b \times \partial_\epsilon G^{A}(\epsilon) - \hat{Q}_a\partial_\epsilon G^{R}(\epsilon)\hat{\jmath}_b G^{<}(\epsilon)]. \tag{A13}$$

For $\hat{Q}_a = \hat{\jmath}_a$, the current-current correlation function gives the well-known dc conductivity formula

$$\sigma_{ab} = -\frac{\hbar}{2\pi V}\int_{-\infty}^{\infty} d\epsilon \mathrm{Tr}[\hat{\jmath}_a G^{<}\hat{\jmath}_b\partial_\epsilon G^{A} - \hat{\jmath}_a\partial_\epsilon G^{R}\hat{\jmath}_b G^{<}], \tag{A14}$$

with V being volume of the sample. Similarly, for $\hat{Q}_a\to\hat{s}_a$, Eq. (A12) gives response of the spin density to dc electric field, characterized by the torkance tensor

$$\tau_{ab} = -\frac{\hbar}{2\pi V}\int_{-\infty}^{\infty} d\epsilon \mathrm{Tr}\big[\hat{s}_a G^{<}\hat{\jmath}_b\partial_\epsilon G^{A} - \hat{s}_a\partial_\epsilon G^{R}\hat{\jmath}_b G^{<}\big]. \tag{A15}$$

The charge current and current-induced spin polarization are given by $J_a = \sigma_{ab}E_b$ and $\Delta s_a = \tau_{ab}E_b$, respectively.

APPENDIX B: DERIVATION FOR THE RESPONSE FUNCTIONS

For a system described by the Hamiltonian

$$\mathcal{H}(\boldsymbol{k}) = \boldsymbol{d}_{\boldsymbol{k}}\cdot\hat{\boldsymbol{\sigma}}, \tag{B1}$$

where $\hat{\boldsymbol{\sigma}}$ is the vector of spin Pauli matrix, we have

$$\hat{s}_a = \frac{\hbar}{2}\frac{\partial\mathcal{H}(\boldsymbol{k})}{\partial d_{\boldsymbol{k},a}} = \frac{\hbar}{2}\sum_\mu \delta_{\mu,a}\hat{\sigma}_\mu, \tag{B2}$$

$$\hat{\jmath}_b = -e\frac{\partial\mathcal{H}(\boldsymbol{k})}{\hbar\partial k_b} = -\frac{e}{\hbar}\sum_\mu \frac{\partial d_{\boldsymbol{k},\mu}}{\partial k_b}\hat{\sigma}_\mu. \tag{B3}$$

Therefore, by noting

$$\xi^{\mu a}_{\boldsymbol{k},j} = -\frac{e\partial d_{\boldsymbol{k},\mu}}{\hbar\partial k_a}\delta_{j,1} + \frac{\hbar}{2}\delta_{\mu,a}\delta_{j,2}, \tag{B4}$$

the conductivity and torkance tensors can be combined into a unified formula as

$$\chi_{j,ab} = -\frac{\hbar}{2\pi V}\int_{-\infty}^{\infty} d\epsilon \sum_{\boldsymbol{k}\mu\nu}\xi^{\mu a}_{\boldsymbol{k},j}\xi^{\nu b}_{\boldsymbol{k},1}\mathrm{Tr}[\hat{\sigma}_\mu G^{<}(\epsilon) \times \hat{\sigma}_\nu\partial_\epsilon G^{A}(\epsilon) - \hat{\sigma}_\mu\partial_\epsilon G^{R}(\epsilon)\hat{\sigma}_\nu G^{<}(\epsilon)]. \tag{B5}$$

The relevant retarded/advanced Green's function is determined by

$$G^{R/A} = \sum_\eta \frac{|\psi_{\boldsymbol{k},\eta}\rangle\langle\psi_{\boldsymbol{k},\eta}|}{\epsilon-\varepsilon_{\boldsymbol{k},\eta}\pm i\Gamma}. \tag{B6}$$

Substituting the retarded and advanced Green's functions into Eq. (B5) yields

$$\chi_{j,ab} = \frac{\hbar}{2\pi V}\sum_{\boldsymbol{k}\eta\eta',\mu\nu}\xi^{\mu a}_{\boldsymbol{k},j}\xi^{\nu b}_{\boldsymbol{k},1}\int_{-\infty}^{\infty} d\epsilon f(\epsilon)\left(\frac{1}{\epsilon-\varepsilon_{\boldsymbol{k},\eta}-i\Gamma}-\frac{1}{\epsilon-\varepsilon_{\boldsymbol{k},\eta}+i\Gamma}\right) \times\partial_\epsilon\left(\frac{\langle\psi_{\boldsymbol{k},\eta}|\hat{\sigma}_\mu|\psi_{\boldsymbol{k},\eta'}\rangle\langle\psi_{\boldsymbol{k},\eta'}|\hat{\sigma}_\nu|\psi_{\boldsymbol{k},\eta}\rangle}{\epsilon-\varepsilon_{\boldsymbol{k},\eta'}+i\Gamma}-\frac{\langle\psi_{\boldsymbol{k},\eta}|\hat{\sigma}_\nu|\psi_{\boldsymbol{k},\eta'}\rangle\langle\psi_{\boldsymbol{k},\eta'}|\hat{\sigma}_\mu|\psi_{\boldsymbol{k},\eta}\rangle}{\epsilon-\varepsilon_{\boldsymbol{k},\eta'}-i\Gamma}\right). \tag{B7}$$

According to $\eta'=\eta$ and $\eta'\neq\eta$, we can divide the response functions into the intraband and interband contributions

$$\chi^{\mathrm{intra}}_{j,ab} = -\frac{\hbar}{V}\sum_{\boldsymbol{k}\eta,\mu\nu}\frac{\partial f(\varepsilon_{\boldsymbol{k},\eta})}{\partial\varepsilon_{\boldsymbol{k},\eta}}\xi^{\mu a}_{\boldsymbol{k},j}\xi^{\nu b}_{\boldsymbol{k},1}\langle\psi_{\boldsymbol{k},\eta}|\hat{\sigma}_\mu|\psi_{\boldsymbol{k},\eta}\rangle\langle\psi_{\boldsymbol{k},\eta}|\hat{\sigma}_\nu|\psi_{\boldsymbol{k},\eta}\rangle\frac{1}{\Gamma}, \tag{B8}$$

$$\chi^{\mathrm{inter}}_{j,ab} = -\frac{i\hbar}{V}\sum_{\boldsymbol{k}\eta,\mu\nu}\xi^{\mu a}_{\boldsymbol{k},j}\xi^{\nu b}_{\boldsymbol{k},1}f(\varepsilon_{\boldsymbol{k},\eta})\left[\frac{\langle\psi_{\boldsymbol{k},\eta}|\hat{\sigma}_\mu|\psi_{\boldsymbol{k},\bar{\eta}}\rangle\langle\psi_{\boldsymbol{k},\bar{\eta}}|\hat{\sigma}_\nu|\psi_{\boldsymbol{k},\eta}\rangle}{(\varepsilon_{\boldsymbol{k},\eta}-\varepsilon_{\boldsymbol{k},\bar{\eta}}+i\Gamma)^2}-\frac{\langle\psi_{\boldsymbol{k},\eta}|\hat{\sigma}_\nu|\psi_{\boldsymbol{k},\bar{\eta}}\rangle\langle\psi_{\boldsymbol{k},\bar{\eta}}|\hat{\sigma}_\mu|\psi_{\boldsymbol{k},\eta}\rangle}{(\varepsilon_{\boldsymbol{k},\eta}-\varepsilon_{\boldsymbol{k},\bar{\eta}}-i\Gamma)^2}\right], \tag{B9}$$

where $\bar{\eta} \equiv -\eta$ and we have used the identity

$$\frac{1}{\epsilon - \varepsilon_{\boldsymbol{k},\eta} - i\Gamma} = P\frac{1}{\epsilon - \varepsilon_{\boldsymbol{k},\eta}} + i\pi\delta\big(\epsilon - \varepsilon_{\boldsymbol{k},\eta}\big). \tag{B10}$$

By defining the angle

$$\tan\vartheta_{\boldsymbol{k}} = \frac{\Gamma}{|\varepsilon_{\boldsymbol{k},\eta} - \varepsilon_{\boldsymbol{k},\bar{\eta}}|}, \tag{B11}$$

we can reexpress $\chi^{\text{inter}}_{j,ab} = \chi^{\text{inter},+}_{j,ab} + \chi^{\text{inter},-}_{j,ab}$, with

$$\begin{aligned}\chi^{\text{inter},+}_{j,ab} &= -\frac{\hbar}{V}\sum_{\boldsymbol{k}\eta,\mu\nu} f(\varepsilon_{\boldsymbol{k},\eta})\xi^{\mu a}_{\boldsymbol{k},j}\xi^{\nu b}_{\boldsymbol{k},1}T^{\eta,+}_{\boldsymbol{k},\mu\nu}\cos^2\vartheta_{\boldsymbol{k}}\sin 2\vartheta_{\boldsymbol{k}},\\ \chi^{\text{inter},-}_{j,ab} &= -\frac{\hbar}{V}\sum_{\boldsymbol{k}\eta,\mu\nu} f(\varepsilon_{\boldsymbol{k},\eta})\xi^{\mu a}_{\boldsymbol{k},j}\xi^{\nu b}_{\boldsymbol{k},1}T^{\eta,-}_{\boldsymbol{k},\mu\nu}\cos^2\vartheta_{\boldsymbol{k}}\cos 2\vartheta_{\boldsymbol{k}},\end{aligned} \tag{B12}$$

where

$$T^{\eta,+}_{\boldsymbol{k},\mu\nu} = \eta\left(\left\langle\frac{\partial\psi_{\boldsymbol{k},\eta}}{\partial d_{\boldsymbol{k},\mu}}\middle|\frac{\partial\psi_{\boldsymbol{k},\eta}}{\partial d_{\boldsymbol{k},\nu}}\right\rangle + \left\langle\frac{\partial\psi_{\boldsymbol{k},\eta}}{\partial d_{\boldsymbol{k},\nu}}\middle|\frac{\partial\psi_{\boldsymbol{k},\eta}}{\partial d_{\boldsymbol{k},\mu}}\right\rangle\right), \tag{B13}$$

$$T^{\eta,-}_{\boldsymbol{k},\mu\nu} = i\left(\left\langle\frac{\partial\psi_{\boldsymbol{k},\eta}}{\partial d_{\boldsymbol{k},\mu}}\middle|\frac{\partial\psi_{\boldsymbol{k},\eta}}{\partial d_{\boldsymbol{k},\nu}}\right\rangle - \left\langle\frac{\partial\psi_{\boldsymbol{k},\eta}}{\partial d_{\boldsymbol{k},\nu}}\middle|\frac{\partial\psi_{\boldsymbol{k},\eta}}{\partial d_{\boldsymbol{k},\mu}}\right\rangle\right). \tag{B14}$$

By the wavefunction

$$|\psi_{\boldsymbol{k},\eta}\rangle = \frac{1}{\sqrt{2|\boldsymbol{d}_{\boldsymbol{k}}|(|\boldsymbol{d}_{\boldsymbol{k}}| - \eta d_{\boldsymbol{k},z})}}\begin{pmatrix} d_{\boldsymbol{k},x} - id_{\boldsymbol{k},y} \\ \eta|\boldsymbol{d}_{\boldsymbol{k}}| - d_{\boldsymbol{k},z}\end{pmatrix}, \tag{B15}$$

we can obtain for

$$T^{\eta,-}_{\boldsymbol{k},\mu\nu} = -\eta\frac{\varepsilon^{\mu\nu\gamma}d_{\boldsymbol{k},\gamma}}{2|\boldsymbol{d}_{\boldsymbol{k}}|^3}, \tag{B16}$$

$$T^{\eta,+}_{\boldsymbol{k},\mu\nu} = -\eta\frac{d_{\boldsymbol{k},\mu}d_{\boldsymbol{k},\nu}}{2|\boldsymbol{d}_{\boldsymbol{k}}|^4}. \tag{B17}$$

APPENDIX C: ANALYSIS FOR THE INTRABAND RESPONSE COEFFICIENTS

For the magnetic semi-Dirac semimetals, according to the symmetry analysis, we find that the transverse torkance here can only come from the mixed BC. As $d_{\boldsymbol{k},x(y)}$ is even (odd) in k_x (k'_y), the parity of a nonzero $\partial d_{\boldsymbol{k},\nu}/\partial k_b$ about k_b is opposite to $d_{\boldsymbol{k},\nu}$, making $d_{\boldsymbol{k},\nu}\partial d_{\boldsymbol{k},\nu}/\partial k_b$ always odd with respect to k_b. Only when the parity of $d_{\boldsymbol{k},\mu}\xi^{\mu a}_{\boldsymbol{k},j}$ is the same as $d_{\boldsymbol{k},\nu}\partial d_{\boldsymbol{k},\nu}/\partial k_b$, which requires $a = b$, can Eq. (4) of the main text survive the integral over $\boldsymbol{k}$. Consequently, $\chi^{\text{intra}}_{j,ab}$ vanishes for $a \neq b$. As compared to Eqs. (4) and (5) of the main text, the symmetry of the integral kernel of $\chi^{\text{inter},+}_{j,ab}$ with respect to $\boldsymbol{k}$ is the same as $\chi^{\text{intra}}_{j,ab}$, such that $\chi^{\text{inter},+}_{j,ab} = 0$ if $a \neq b$.

The intraband response of the spin density to the charge current, originating from the electron states on the Fermi surface, is extrinsic and can be scaled by $\chi^{\text{intra}}_{2,ay}/\sigma_{yy} = -\delta_{a,y}\hbar^2/(2\upsilon e)$ and $\chi^{\text{intra}}_{2,ax}/\sigma_{xx} = 0$, whose behavior can be understood intuitively by a picture resembling the charge current in solids. As illustrated by Fig. 1 and Fig. 4 of the main text, due to the special spin-momentum locking, the signs of the x (y) component of the spin are identical (opposite) for carriers with opposite momentum. As a result, the forward and backward channel numbers are added (subtracted) to contribute to the polarization in the x (y) direction. This also explains why in the equilibrium there is finite (no) magnetization in the x (y) direction. With the electric field turned on, the carrier number will increase in one direction and decrease in the opposite, leading to nonequilibrium distribution of the carriers along the electric field. If the electric field is along direction y, the number difference between the forward and backward moving carriers will result in a net y spin density. However, for the x direction, the decrease of the spin density on the backward channels will be compensated by the increase on the forward, making the total spin density unchanged. Consequently, $\chi^{\text{intra}}_{2,yy}$ can be finite but $\chi^{\text{intra}}_{2,xx}$ is vanishing, which is consistent with the scaled relation above.

[1] G. Prenat, K. Jabeur, G. Di Pendina, O. Boulle, and G. Gaudin, *Spintronics-based Computing*, edited by W. Zhao and G. Prenat (Springer International Publishing, Cham, 2015), pp. 145–157.

[2] A. Manchon, J. Železný, I. M. Miron, T. Jungwirth, J. Sinova, A. Thiaville, K. Garello, and P. Gambardella, Rev. Mod. Phys. **91**, 035004 (2019).

[3] A. Chernyshov, M. Overby, X. Liu, J. K. Furdyna, Y. Lyanda-Geller, and L. P. Rokhinson, Nat. Phys. **5**, 656 (2009).

[4] M. Endo, F. Matsukura, and H. Ohno, Appl. Phys. Lett. **97**, 222501 (2010).

[5] D. Fang, H. Kurebayashi, J. Wunderlich, K. Výborný, L. P. Zârbo, R. P. Campion, A. Casiraghi, B. L. Gallagher, T. Jungwirth, and A. J. Ferguson, Nat. Nanotechnol. **6**, 413 (2011).

[6] I. M. Miron, T. Moore, H. Szambolics, L. D. Buda-Prejbeanu, S. Auffret, B. Rodmacq, S. Pizzini, J. Vogel, M. Bonfim, A. Schuhl, and G. Gaudin, Nat. Mater. **10**, 419 (2011).

[7] K. Garello, I. M. Miron, C. O. Avci, F. Freimuth, Y. Mokrousov, S. Blügel, S. Auffret, O. Boulle, G. Gaudin, and P. Gambardella, Nat. Nanotechnol. **8**, 587 (2013).

[8] F. Freimuth, S. Blügel, and Y. Mokrousov, Phys. Rev. B **90**, 174423 (2014).

[9] I. Mihai Miron, G. Gaudin, S. Auffret, B. Rodmacq, A. Schuhl, S. Pizzini, J. Vogel, and P. Gambardella, Nat. Mater. **9**, 230 (2010).

[10] I. M. Miron, K. Garello, G. Gaudin, P.-J. Zermatten, M. V. Costache, S. Auffret, S. Bandiera, B. Rodmacq, A. Schuhl, and P. Gambardella, Nature (London) **476**, 189 (2011).

[11] L. Liu, O. J. Lee, T. J. Gudmundsen, D. C. Ralph, and R. A. Buhrman, Phys. Rev. Lett. **109**, 096602 (2012).

[12] H. Li, H. Gao, L. P. Zârbo, K. Výborný, X. Wang, I. Garate, F. Doğan, A. Čejchan, J. Sinova, T. Jungwirth, and A. Manchon, Phys. Rev. B **91**, 134402 (2015).

[13] P. Wadley, B. Howells, J. Železný, C. Andrews, V. Hills, R. P. Campion, V. Novák, K. Olejník, F. Maccherozzi, S. S. Dhesi, S. Y. Martin, T. Wagner, J. Wunderlich, F. Freimuth, Y. Mokrousov, J. Kuneš, J. S. Chauhan, M. J. Grzybowski, A. W. Rushforth, K. W. Edmonds *et al.*, Science **351**, 587 (2016).

[14] M.-X. Deng, M. Zhong, S.-H. Zheng, J.-M. Qiu, M. Yang, and R.-Q. Wang, J. Appl. Phys. **119**, 073903 (2016).
[15] R. Ramaswamy, J. M. Lee, K. Cai, and H. Yang, Appl. Phys. Rev. **5**, 031107 (2018).
[16] J.-Y. Li, R.-Q. Wang, M.-X. Deng, and M. Yang, Phys. Rev. B **99**, 155139 (2019).
[17] H. Wu, P. Zhang, P. Deng, Q. Lan, Q. Pan, S. A. Razavi, X. Che, L. Huang, B. Dai, K. Wong, X. Han, and K. L. Wang, Phys. Rev. Lett. **123**, 207205 (2019).
[18] E. Grimaldi, V. Krizakova, G. Sala, F. Yasin, S. Couet, G. Sankar Kar, K. Garello, and P. Gambardella, Nat. Nanotechnol. **15**, 111 (2020).
[19] L. Zhu, D. C. Ralph, and R. A. Buhrman, Appl. Phys. Rev. **8**, 031308 (2021).
[20] C. Song, R. Zhang, L. Liao, Y. Zhou, X. Zhou, R. Chen, Y. You, X. Chen, and F. Pan, Prog. Mater. Sci. **118**, 100761 (2021).
[21] Y. Takeuchi, Y. Yamane, J.-Y. Yoon, R. Itoh, B. Jinnai, S. Kanai, J. Ieda, S. Fukami, and H. Ohno, Nat. Mater. **20**, 1364 (2021).
[22] L. Liu, C.-F. Pai, Y. Li, H. W. Tseng, D. C. Ralph, and R. A. Buhrman, Science **336**, 555 (2012).
[23] C. O. Avci, K. Garello, M. Gabureac, A. Ghosh, A. Fuhrer, S. F. Alvarado, and P. Gambardella, Phys. Rev. B **90**, 224427 (2014).
[24] M. Jamali, K. Narayanapillai, X. Qiu, L. M. Loong, A. Manchon, and H. Yang, Phys. Rev. Lett. **111**, 246602 (2013).
[25] A. R. Mellnik, J. S. Lee, A. Richardella, J. L. Grab, P. J. Mintun, M. H. Fischer, A. Vaezi, A. Manchon, E.-A. Kim, N. Samarth, and D. C. Ralph, Nature (London) **511**, 449 (2014).
[26] T. Gao, A. Qaiumzadeh, H. An, A. Musha, Y. Kageyama, J. Shi, and K. Ando, Phys. Rev. Lett. **121**, 017202 (2018).
[27] L. Zhu, D. C. Ralph, and R. A. Buhrman, Phys. Rev. Lett. **122**, 077201 (2019).
[28] T. Nan, T. J. Anderson, J. Gibbons, K. Hwang, N. Campbell, H. Zhou, Y. Q. Dong, G. Y. Kim, D. F. Shao, T. R. Paudel, N. Reynolds, X. J. Wang, N. X. Sun, E. Y. Tsymbal, S. Y. Choi, M. S. Rzchowski, Y. B. Kim, D. C. Ralph, and C. B. Eom, Proc. Natl. Acad. Sci. **116**, 16186 (2019).
[29] J. Zhou, X. Shu, W. Lin, D. F. Shao, S. Chen, L. Liu, P. Yang, E. Y. Tsymbal, and J. Chen, Adv. Mater. **33**, 2007114 (2021).
[30] P. W. Swatek, X. Hang, Y. Fan, W. Jiang, H. Yun, D. Lyu, D. Zhang, T. J. Peterson, P. Sahu, O. J. Benally, Z. Cresswell, J. Liu, R. Pahari, D. Kukla, T. Low, K. A. Mkhoyan, and J.-P. Wang, Phys. Rev. Mater. **6**, 074206 (2022).
[31] H. Kurebayashi, J. Sinova, D. Fang, A. C. Irvine, T. D. Skinner, J. Wunderlich, V. Novák, R. P. Campion, B. L. Gallagher, E. K. Vehstedt, L. P. Zârbo, K. Výborný, A. J. Ferguson, and T. Jungwirth, Nat. Nanotechnol. **9**, 211 (2014).
[32] J.-P. Hanke, F. Freimuth, C. Niu, S. Blügel, and Y. Mokrousov, Nat. Commun. **8**, 1479 (2017).
[33] C. Niu, J.-P. Hanke, P. M. Buhl, H. Zhang, L. Plucinski, D. Wortmann, S. Blügel, G. Bihlmayer, and Y. Mokrousov, Nat. Commun. **10**, 3179 (2019).
[34] T. J. Peterson, M. DC, Y. Fan, J. Chen, D. Zhang, H. Li, P. Swatek, J. Garcia-Barriocanal, and J.-P. Wang, Phys. Rev. Mater. **5**, 045003 (2021).
[35] T. Jungwirth, Q. Niu, and A. H. MacDonald, Phys. Rev. Lett. **88**, 207208 (2002).
[36] N. Nagaosa, J. Sinova, S. Onoda, A. H. MacDonald, and N. P. Ong, Rev. Mod. Phys. **82**, 1539 (2010).
[37] S. Murakami, N. Nagaosa, and S.-C. Zhang, Science **301**, 1348 (2003).
[38] J. Sinova, D. Culcer, Q. Niu, N. A. Sinitsyn, T. Jungwirth, and A. H. MacDonald, Phys. Rev. Lett. **92**, 126603 (2004).
[39] J. Sinova, S. O. Valenzuela, J. Wunderlich, C. H. Back, and T. Jungwirth, Rev. Mod. Phys. **87**, 1213 (2015).
[40] A. Kalitsov, S. A. Nikolaev, J. Velev, M. Chshiev, and O. Mryasov, Phys. Rev. B **96**, 214430 (2017).
[41] A. S. Rodin, A. Carvalho, and A. H. Castro Neto, Phys. Rev. Lett. **112**, 176801 (2014).
[42] A. Kobayashi, Y. Suzumura, F. Piéchon, and G. Montambaux, Phys. Rev. B **84**, 075450 (2011).
[43] Y. Wu, Opt. Express **22**, 1906 (2014).
[44] P. Dietl, F. Piéchon, and G. Montambaux, Phys. Rev. Lett. **100**, 236405 (2008).
[45] A. Zarifi and M. Zare, J. Magn. Magn. Mater. **536**, 168117 (2021).
[46] S. Banerjee, arXiv:1508.05145.
[47] V. Pardo and W. E. Pickett, Phys. Rev. Lett. **102**, 166803 (2009).
[48] S. Banerjee, R. R. P. Singh, V. Pardo, and W. E. Pickett, Phys. Rev. Lett. **103**, 016402 (2009).
[49] H. Huang, Z. Liu, H. Zhang, W. Duan, and D. Vanderbilt, Phys. Rev. B **92**, 161115(R) (2015).
[50] A. Mawrie and B. Muralidharan, Phys. Rev. B **99**, 075415 (2019).
[51] J.-N. Chen, Y.-Y. Yang, Y.-L. Zhou, Y.-J. Wu, H.-J. Duan, M.-X. Deng, and R.-Q. Wang, Phys. Rev. B **105**, 085124 (2022).
[52] S. Mondal and S. Basu, Phys. Rev. B **105**, 235441 (2022).
[53] V. Gritsev and A. Polkovnikov, Proc. Natl. Acad. Sci. **109**, 6457 (2012).
[54] K. Saha, Phys. Rev. B **94**, 081103(R) (2016).
[55] A. Mawrie and B. Muralidharan, Phys. Rev. B **100**, 081403(R) (2019).
[56] G. Xu, H. Weng, Z. Wang, X. Dai, and Z. Fang, Phys. Rev. Lett. **107**, 186806 (2011).
[57] M.-X. Deng, W. Luo, R.-Q. Wang, L. Sheng, and D. Y. Xing, Phys. Rev. B **96**, 155141 (2017).
[58] B. Q. Lv, T. Qian, and H. Ding, Rev. Mod. Phys. **93**, 025002 (2021).
[59] Y.-L. Zhou, H.-J. Duan, Y. J. Wu, M.-X. Deng, L. Wang, D. Culcer, and R.-Q. Wang, Phys. Rev. B **105**, 075415 (2022).